Interplay between chemical reactions and transport in structured spaces

Zoran Konkoli*
Department of Applied Physics, Chalmers University of Technology and Göteborg University, SE-412 96 Göteborg, Sweden
(Received 8 April 2005; revised manuscript received 2 June 2005; published 27 July 2005)

The main motivation behind this study is to understand the interplay between the reactions and transport in a geometries that are not compact. Typical examples of compact geometries are a box or a sphere. A network made of containers $C_1, C_2, \ldots, C_N$ and tubes is an example of the space that is structured and noncompact. In containers, particles react with the rate λ. Tubes connecting containers allow for the exchange of chemicals with the transport rate D. A situation is considered where a number of reactants is small and kinetics is noise dominated. A method is presented that can be used to calculate the average and higher moments of the reaction time. A number of different chemical reactions are studied and their performance compared in various ways. Two schemes are discussed in general, the reaction on a fixed geometry ensemble (ROGE) and the geometry on a fixed reaction ensemble, examples are given in the ROGE case. The most important findings are as follows. (i) There is a large number of reactions that run faster in a networklike geometry. Such reactions contain antagonistic catalytic influences in the intermediate stages of a reaction scheme that are best dealt with in a networklike structure. (ii) Antagonistic catalytic influences are hard to identify since they are strongly connected to the pattern of injected molecules (inject pattern) and depend on the choice of molecules that have to be synthesized at the end (task pattern). (iii) The reaction time depends strongly on the details of the inject and task patterns.

DOI: 10.1103/PhysRevE.72.011917 PACS number(s): 82.39.Rt, 87.17.Aa, 05.40.−a

I. INTRODUCTION

The goal of the present study is to impact some progress in understanding the interplay between the reactions and transport in structured spaces. There are many questions one could ask. This study focuses on two. First, assuming that the spatial structure is fixed, which reaction scheme would draw the most benefit from it, for example, in terms of speed (smaller execution time) or better timing (reduction of noise level)? Second, given the chemical reaction, what is the topology that is mostly suited for it?

The situation considered here is shown in Fig. 1. The goal is to investigate the setup where reactions happen in the specific regions of space and reactants move among these regions. The simplest way of achieving such a setup is to consider the chemical reactions in containers that are connected by tubes, as shown in the figure.

The particular model proposed here is influenced by several lines of research. The setup of the reaction schemes is inspired by the work done on the prebiotic evolution, genome-based evolution and random reaction networks [1–8], and diffusion-controlled reactions in the bulk phase [9–14] and in restricted geometries [15–18]. The geometrical setup of the model is motivated by the experimental studies given in Refs. [19–25] and the theoretical study of the reaction-diffusion neuron and enzymatic neuron [26–32].

For simplicity reasons, the details, of both the chemical reactions and transport, are neglected to a large extent. It is assumed that reactants are pointlike objects with no structure. The two most important time scales are traced in the model. The reaction rate λ describes how fast molecules react in containers. The transport rate D governs the exchange of the chemicals among containers. In order to gain some understanding of the differences between the compact and structured geometries, depicted in panels (a) and (b) of Fig. 1, one simply has to study variations of a reaction dynamics in the networklike structure (c) as the transport rate changes from $D \sim \lambda$ toward $D \gg \lambda$. This is the main idea of the paper.

To understand in which ways a particular shape of the reaction volume influences the chemical kinetics (and vise versa) a large number of chemical reactions are compared. Two ensembles are discussed in general. In the first case, the reaction scheme is kept fixed, while the geometry of the network is allowed to change. This type of ensemble will be referred to as the geometry on the (fixed) reaction ensemble (GORE). The geometries are different and they are sampled by changing the size of the containers and the length of the tubes. In the second case the geometry of the network is kept fixed, while the reaction scheme is subject to a change. This type of the ensemble will be referred to as the reaction on the (fixed) geometry ensemble (ROGE). Examples will be given for the ROGE case only.

What is the measure of the good performance for a chemical reaction? In here, the focus will be on the time related issues such as the length of the catalytic cycles. The setup presented here allows for the consideration of other performance criteria but these are omitted due to the simplicity reasons. The time needed for a reaction to finish, $\mathcal{T}$, is a stochastic variable. All information about $\mathcal{T}$ is obtained in the distribution function $\Phi(t)$ that describes its statistics. In practice it is very hard to find $\Phi(t)$ for a general reaction scheme. It is more fruitful to characterize $\Phi(t)$ in terms of a few variables and in this work we use the average $\tau = \int_0^\infty t\Phi(t)dt$.

The paper is organized as follows. In Secs. II and III the reaction-diffusion model is defined in detail, and in Sec. IV

*Electronic address: zorank@fy.chalmers.se

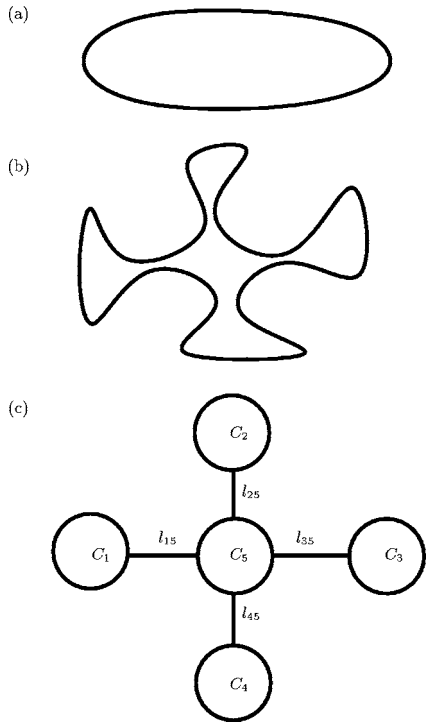

FIG. 1. The goal is to understand how reaction dynamics alters when geometry of the system changes from compact, shown in panel (a), toward noncompact (structured), shown in panel (b). This can be done by studying one system, depicted in panel (c). Panel (c) shows how to model geometry in panel (b) in terms of network consisting of containers and tubes. When $D \sim \lambda$ the reaction dynamics in panels (b) and (c) should exhibit some similarities. For $D \gg \lambda$ one expects the same for the structures (a) and (c).

an overview of the methods for solving the master equation is given. The method of doing a computer simulation is reviewed first. The method of finding moments of the time length of the catalytic cycles is discussed in detail in the Sec. V. A few simple reactions are discussed in Sec. VI where it is shown how to compare vastly different reaction schemes. Section VII contains analysis of the ROGE ensemble made from a two container network, two particle types, all possible reactions, and a full set of inject-task patterns. The conclusions and outlook are given in Sec. VIII.

II. REACTIONS OCCUR IN A NETWORK STRUCTURE

The reaction-diffusion model is defined as follows. Consider the set of containers C_i connected in a particular way by tubes with lengths $l_{i,j}$; $i,j=1,\ldots,N$. It is possible that some containers are not connected. An example of such a structure is given in Fig. 1. The containers harbor molecules X_α; $\alpha=1,2,\ldots,M$. Molecules are allowed to react only when in the same container (provided there is a reaction they participate in) with the rate λ. Molecule X_α moves from container C_i to container C_j with a rate of D_{ij}^α. For simplicity reasons it is assumed that $D_{ij}^\alpha=D$ if the link between container i and j exists and equals zero otherwise.

It is very common to model diffusion-controlled reactions by using a similar type of dynamics. Instead of the network structure one uses regular lattice, for reviews see Refs. [9–14]. The lattice models have the three most important characteristics: the lattice is a highly regular structure (number of neighbors is well defined), infinite lattices are of the major concern, and when the lattice size gets large the calculations become technical and only simple models can be solved. Here, the focus is on highly irregular, small networks, with more complicated reaction schemes.

Structures like the ones shown in Fig. 1 can be found in the interior of the living cells. A few examples are golgi, mitochondria, and endoplasmic reticulum. Mapping is not exact, but there is a rough similarity. In the living cell N can vary from few containers (protein complexes), towards values that are in between 10 and 100 (golgi, mitochondrion). Also, the number of the molecule types M can be very few towards very large numbers of the order of 100 or more. Please see Refs. [33–36] for additional details.

With assumptions at hand, to describe the system at any time instant, it is sufficient to track the number of particles in each container. The conformation of system $\boldsymbol{c}$ is specified as an occupancy of the containers

$$\boldsymbol{c} = (\boldsymbol{n}_1,\ldots,\boldsymbol{n}_i,\ldots,\boldsymbol{n}_N), \tag{1}$$

where vectors $\boldsymbol{n}_i$ $i=1,\ldots,N$ describe the particle content of each container

$$\boldsymbol{n}_i = (n_{1,i},\ldots,n_{\alpha,i},\ldots,n_{M,i}) \tag{2}$$

with $n_{\alpha,i}=0,1,2,\ldots,\infty$ for $\alpha=1,\ldots,M$ and $i=1,\ldots,N$. The system makes random transitions between various configurations.

For computational convenience, the very simple type of a reaction scheme will be considered

$$X_\alpha \xrightarrow{\pm X_\gamma} X_\beta. \tag{3}$$

The reaction graph is specified by the reactivity matrix $\boldsymbol{\Lambda}$. If reaction $X_\alpha \to X_\beta$ is allowed $\Lambda_{\alpha,\beta}=1$ and equals zero otherwise. The catalysis information is stored into matrix $K_{\alpha,\beta}$ where $K_{\alpha,\beta}=\pm\gamma$ if X_γ is catalyst (+) or inhibitor (−) for $X_\alpha \to X_\beta$ reaction. $K_{\alpha,\beta}=0$ indicates that the reaction does not have a catalyst nor an inhibitor.

The reaction rate for the reaction $X_\alpha \to X_\beta$ in container C_i is given by

$$\lambda_{\alpha,\beta}^i(\boldsymbol{n}_i) = \lambda\Lambda_{\alpha,\beta}\begin{cases} 1 & \kappa=0 \\ \xi & \kappa>0, \quad n_{\kappa,i} > \delta_{\kappa,\alpha} \\ \dfrac{1}{\xi} & \kappa<0, \quad n_{|\kappa|,i} > \delta_{|\kappa|,\alpha}. \end{cases} \tag{4}$$

$\delta_{\alpha,\beta}$ is a Kronecker delta function, $\xi>1$ denotes the catalysis enhancement factor, and $\kappa=K_{\alpha,\beta}$. The condition $n_{\kappa,i}>\delta_{\kappa,\alpha}$ ensures that there is no self catalysis for a reaction of the type

$$X_\alpha \xrightarrow{X_\alpha} X_\beta \tag{5}$$

when there is only one X_α present in the container. One needs at least two X_α in order to feel catalytic influence of X_α on the reaction given in (5).

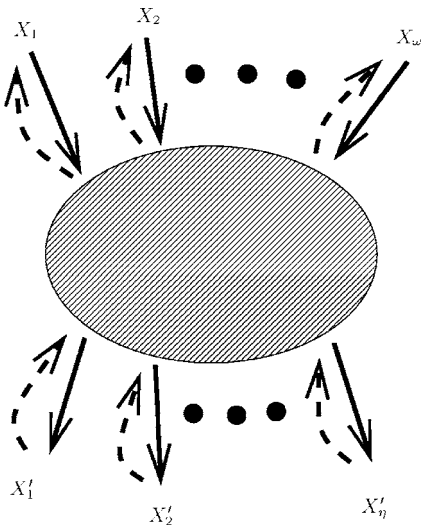

FIG. 2. The most general form of a reaction graph considered.

III. REACTION TIME CAN BE DEFINED BY INTRODUCING INJECT AND TASK PATTERNS

The most general reaction graph one can consider is shown in Fig. 2. The graph indicates that cell machinery converts molecules $X_1,\ldots,X_\omega$ into molecules $X_1',X_2',\ldots,X_\eta'$. The shaded area in the middle denotes the intermediate reaction steps that involve an arbitrary set of reactions between the molecules already shown in the graph. An additional particle types may appear in the shaded region. It is possible to define the speed of a reaction as the time needed for the predetermined set of output molecules $X_1',X_2',\ldots,X_\eta'$ to appear, provided only the input molecules were present initially in the system.

In addition to the reaction scheme given in Eq. (3) one has to specify

$$\boldsymbol{\iota}=(\iota_1,\iota_2,\ldots,\iota_\omega),\quad \boldsymbol{\pi}=(\pi_1,\pi_2,\ldots,\pi_\eta). \tag{6}$$

The vector $\boldsymbol{\iota}$ contains a list of molecules injected, their number, and the location (container) where they are inserted into the system. $\boldsymbol{\pi}$ defines a list of tasks indicating which molecules should be synthesized, how many, and in which container they should appear.

Every time a certain task is accomplished the time when this happens is stored. These times are arranged in the vector

$$\boldsymbol{\mathcal{T}}=(\mathcal{T}_1,\mathcal{T}_2,\ldots,\mathcal{T}_\eta) \tag{7}$$

and there is a one to one correspondence between the elements of $\boldsymbol{\pi}$ and $\boldsymbol{\mathcal{T}}$. The vector $\boldsymbol{\mathcal{T}}$ is a stochastic variable and can be described in terms of the distribution function $\Phi(t_1,t_2,\ldots,t_n;\boldsymbol{\iota},\boldsymbol{\pi})$.

Once the task is achieved molecules that were used to accomplish it are removed from the system. This consideration is motivated by the character of the real processes in the living cell. A typical example is the conversion of the substrate molecule through action of an enzyme (e.g., as in the citric acid cycle in mitochondria) [34]. Also, the molecule removal couples tasks and $\Phi(t_1,t_2,\ldots,t_n;\iota,\pi)$ cannot be factorized into $\Phi_1(t_1)\Phi_2(t_2)\cdots\Phi_n(t_n)$. This implies that whole set of tasks should be considered as one entity. This adds a different dimension into the dynamics.

In practice, it is very hard to obtain a full distribution function and it is more convenient to characterize it in terms of the few lowest moments. In this work we use the average

$$\boldsymbol{\tau}=(\tau_1,\ldots,\tau_k,\ldots,\tau_n). \tag{8}$$

One could also use the variance but this is not done at the moment.

The quadruple consisting of a particular reaction scheme (λ, ξ, $\boldsymbol{\Lambda}$, and $\boldsymbol{K}$), network geometry ($l_{i,j}i$, $j=1,\ldots,N$), inject pattern $\boldsymbol{\iota}$, and list of tasks monitored $\boldsymbol{\pi}$, will be referred to as an *organism*. The organism can be seen as the entity that has to transform a certain number of chemicals into a set of molecules that have to be synthesized at certain places, utilizing the available reaction scheme and geometry.

IV. THE MASTER EQUATION IS SOLVED BY COMPUTER SIMULATION AND MOMENT METHOD

The dynamics of the system defined in the previous section is stochastic and from the rules discussed one can derive a master equation that describes the time evolution of the occupation probabilities $p(\boldsymbol{c},t)$,

$$\dot{p}(\boldsymbol{c},t)=\sum_{\boldsymbol{c}'}R_{\boldsymbol{c},\boldsymbol{c}'}p(\boldsymbol{c}',t)-\sum_{\boldsymbol{c}'}R_{\boldsymbol{c}'\boldsymbol{c}}p(\boldsymbol{c},t), \tag{9}$$

where here and in the following the dot over symbol denotes time derivative. The reaction rates $R_{\boldsymbol{c}'\boldsymbol{c}}$ for $\boldsymbol{c}\to\boldsymbol{c}'$ transition can be easily calculated from the definition of the model. Two numerical strategies are used to solve Eq. (9), the simulation method and procedure developed in here to calculate various moments of the $\Phi(t_1,\ldots,t_n;\boldsymbol{\iota},\boldsymbol{\pi})$.

A. Computer simulation

The master equation is solved by using a minimal process algorithm suggested by Gillespie [37,38]. Given that at the time t the system is in the conformation $\boldsymbol{c}$ the following processes can happen. Transport of particle X_α from C_i to C_j occurs with rates

$$R_{i,j}^{\alpha}(\boldsymbol{c})=D_{i,j}^{\alpha}n_{\alpha,i},\quad \alpha=1,2,\ldots,M,\quad i,j=1,\ldots,N \tag{10}$$

or reactions within containers with rates

$$R_{\alpha,\beta}^{i}(\boldsymbol{c})=\lambda_{\alpha,\beta}^{i}(\boldsymbol{n}_i)n_{\alpha,i}. \tag{11}$$

One also needs the total reaction rate

$$Q(\boldsymbol{c})=\sum_{i,j=1}^{N}\sum_{\alpha=1}^{M}R_{i,j}^{\alpha}(\boldsymbol{c})+\sum_{i=1}^{N}\sum_{\alpha,\beta=1}^{M}R_{\alpha,\beta}^{i}(\boldsymbol{c}) \tag{12}$$

which is used to sample the waiting time $\Delta t=-\ln(1-r)/Q$ where r is a random number drawn uniformly from the interval [0, 1). The probabilities for the process to happen are given by

$$p_{i,j}^{\alpha}=\frac{R_{i,j}^{\alpha}(\boldsymbol{c})}{Q},\quad \alpha=1,\ldots,M,\quad i,j=1,\ldots,N, \tag{13}$$

$$p^i_{\alpha,\beta} = \frac{R^i_{\alpha,\beta}(\boldsymbol{c})}{Q}, \quad i = 1,\ldots,N, \quad \alpha,\beta = 1,\ldots,M. \quad (14)$$

A process is chosen using the linear selection algorithm: First, a random number r' is drawn. After that, the cumulant probabilities are calculated through the loop over all processes. The loop is stopped when the cumulant probability exceeds r' and the last process for which this happened is executed.

B. Moment method

This method relies on the matrix representation of the master equation (9) and cannot be used to treat cases with a large number of containers and particle types (the size of the configuration space grows exponentially). However, the method is exact and should be used when there are enough computation resources. The method is developed in the following section.

V. THE CALCULATION OF THE REACTION TIME MOMENTS

It will be shown how to calculate the moments of the individual components of $\boldsymbol{\tau}$, $\gamma^{(p)}_k \equiv \langle (\tau_k)^p \rangle$, $k=1,\ldots,\eta$ and $p=0,1,2,\ldots,\infty$, where

$$\gamma^{(p)}_k(\boldsymbol{\iota},\boldsymbol{\pi}) = \int_0^\infty t^p \Gamma_k(t;\boldsymbol{\iota},\boldsymbol{\pi})dt. \quad (15)$$

$\Gamma_k(t;\boldsymbol{\iota},\boldsymbol{\pi})$ denotes integrated distribution function for task π_k,

$$\Gamma_k(t;\boldsymbol{\iota},\boldsymbol{\pi}) \equiv \int_0^\infty \Phi(t_1,\ldots,t_n;\boldsymbol{\iota},\boldsymbol{\pi}) \prod_{m=1,\eta}^{m\neq k} dt_m. \quad (16)$$

Please note that the accomplishment of each individual task is influenced by the presence of others since the particles vanish upon the accomplishment of various tasks, and both the index of the task (k) and the full list of tasks being monitored ($\boldsymbol{\pi}$) have to be specified.

It is possible to find a closed expression for the Laplace transform of $\Gamma_k(t;\boldsymbol{\iota},\boldsymbol{\pi})$. The Laplace transform of arbitrary function $F(t)$ is defined as $F(s) \equiv \int_0^\infty \exp(-st)F(t)dt$. $\Gamma_k(s;\boldsymbol{\iota},\boldsymbol{\pi})$ is given by

$$\begin{aligned}\Gamma_k(s;\boldsymbol{\iota},\boldsymbol{\pi}) = &\sum_{\boldsymbol{c}\neq\boldsymbol{\iota}} w(\boldsymbol{c},\pi_k) g(s;\boldsymbol{\iota},\boldsymbol{c},\boldsymbol{\pi}) \\ &+ \sum_{m=1,\eta}^{m\neq k} \sum_{\boldsymbol{c}\neq\boldsymbol{\iota}} w(\boldsymbol{c},\pi_m) g(s;\boldsymbol{\iota},\boldsymbol{c},\boldsymbol{\pi}) \\ &\times \Gamma_k(s;\boldsymbol{c}/\pi_m,\boldsymbol{\pi}/\pi_m), \end{aligned} \quad (17)$$

where the notation used is as follows. The $w(\boldsymbol{c},\pi_k)$ equals one if the task π_k can be accomplished once the system arrives in the state $\boldsymbol{c}$, and equals zero otherwise. In the following, by definition, a state for which one of the $w(\boldsymbol{c},\pi_k)$ with $k=1,\ldots,\eta$ differs from zero will be referred to as a *window* state. Through the window state tasks can be accomplished. $\boldsymbol{c}/\pi_m$ denotes the state immediately after the particles have been taken away once the task π_m was accomplished. Likewise, the symbol $\boldsymbol{\pi}/\pi_m$ denotes a list of tasks being monitored with task π_m omitted $(\pi_1,\ldots,\pi_{m-1},\pi_{m+1},\ldots,\pi_\eta)$. $g(s;\boldsymbol{\iota},\boldsymbol{c},\boldsymbol{\pi})$ is a distribution function for the first passage time into the state $\boldsymbol{c}$ given that the dynamics started from the state $\boldsymbol{\iota}$. Figure 3 is a schematic presentation of the Eq. (17). Please note that Eq. (17) defines $\Gamma_k(s;\boldsymbol{\iota},\boldsymbol{\pi})$ recursively. The number of tasks on the right-hand side of Eq. (17) is smaller by one than the same number on the left-hand side of the equation. When the list of a task is empty $\boldsymbol{\pi}=\boldsymbol{\pi}_0$ and $\boldsymbol{\pi}_0 \equiv (\,)$. The condition $\Gamma_k(s;\boldsymbol{\iota},\boldsymbol{\pi}_0)=0$ stops the recursion.

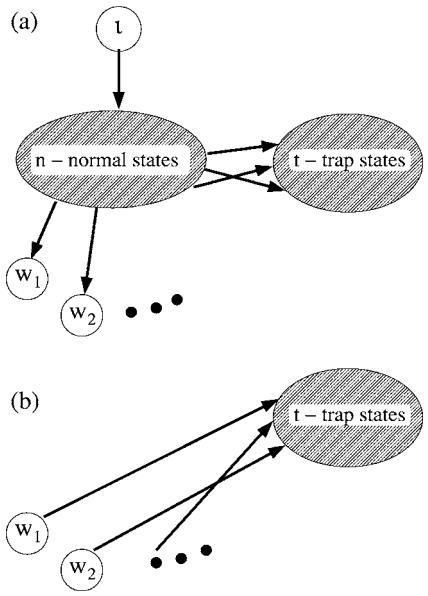

FIG. 3. Panel (a): The structure of the configuration space. Initially the system is in the state $\boldsymbol{\iota}$. Three set of states are distinguished, a set of normal states S_n, a set of trap states S_t, and a set of window states S_w. Panel (b): graphical illustration of the partitioning algorithm.

The Laplace transform of the arrival time distribution function $g(t;\boldsymbol{\iota},\boldsymbol{c},\boldsymbol{\pi})$ is calculated as follows. Given the particular reaction scheme it is possible to construct a master equation (9) that governs the time dependence of the occupation probabilities of each state $p(\boldsymbol{c},t)$, where $\boldsymbol{c}$ has to be accessible from the initial state $\boldsymbol{\iota}$. When calculating the matrix of the transition rates $\boldsymbol{R}$ it is assumed that all window states cannot be left once they are arrived into. Window states are perfectly absorbing. Figure 3 is a graphic representation of this fact. Once $p(\boldsymbol{c},t)$ is found from (9) the passage time distribution function is given by $g(t,\boldsymbol{\iota},\boldsymbol{c},\boldsymbol{\pi}) = \dot{p}(\boldsymbol{c},t)$.

It is useful to arrange both $p(\boldsymbol{c},t)$ and $g(s;\boldsymbol{\iota},\boldsymbol{c},\boldsymbol{\pi})$ into a vectors $\boldsymbol{p}(t)$ and $\boldsymbol{g}(t)$ where notation was simplified a bit since we assume that $\boldsymbol{\iota}$ and $\boldsymbol{\pi}$ are known and fixed. It is useful to rewrite master equation (9) in a matrix form as $\dot{\boldsymbol{p}}(t) = \boldsymbol{R}p(t)$. This equation is solved using the Laplace transform, with initial condition $p(\boldsymbol{c},0) = \delta_{\boldsymbol{c},\boldsymbol{\iota}}$ (δ denotes the Kronecker delta symbol): $s\boldsymbol{p}(s) - \boldsymbol{p}_0 = \boldsymbol{R}p(s)$. Also, in the Laplace transform space one has $s\boldsymbol{p}(s) - \boldsymbol{p}_0 = \boldsymbol{g}(s)$, which directly leads to the equation for the arrival time distribution function

$$s\boldsymbol{g}(s) = \boldsymbol{R}[\boldsymbol{g}(s) + \boldsymbol{p}_0]. \tag{18}$$

In principle, the equation above could be solved as $\boldsymbol{g}(s) = (s - \boldsymbol{R})^{-1}\boldsymbol{p}_0$. However, matrix $\boldsymbol{R}$ has zero eigenvalues and the value of $\boldsymbol{g}(s)$ in the limit $s \to 0$ is ill defined. To avoid such problems Eq. (18) has to be solved in a special way.

It is useful to separate configuration space into three groups: a set of normal (nonwindow) states S_n, a set of trap states S_t, and a set of window states S_w, as shown in Fig. 3. The existence of the trap states is problem dependent. Once the system arrives into these states there is no exit from this space, though such states are not window states. This simply means that it is possible that the set of tasks is never accomplished.

Using the partition of states shown in Fig. 3 leads to the following set of equations:

$$s\boldsymbol{g}_n(s) = \boldsymbol{R}_{nn}[\boldsymbol{g}_n(s) + \boldsymbol{p}_{n,0}], \tag{19}$$

$$s\boldsymbol{g}_t(s) = \boldsymbol{R}_{tn}[\boldsymbol{g}_n(s) + \boldsymbol{p}_{n,0}] + \boldsymbol{R}_{tt}\boldsymbol{g}_t(s), \tag{20}$$

$$s\boldsymbol{g}_w(s) = \boldsymbol{R}_{wn}[\boldsymbol{g}_n(s) + \boldsymbol{p}_{n,0}]. \tag{21}$$

Please note that $\boldsymbol{p}_{t,0}$ and $\boldsymbol{p}_{w,0}$ are zero since, initially, the system is in the state $\boldsymbol{\iota}$ and such a state does not have any components in the S_t and S_w spaces. Given that there is no transition from the trap states into the normal states or window states blocks $\boldsymbol{R}_{nt}$ and $\boldsymbol{R}_{wt}$ are missing in the equations above. Likewise, blocks $\boldsymbol{R}_{ww}$, $\boldsymbol{R}_{nw}$, and $\boldsymbol{R}_{tw}$ are zero since there are no transitions among the window states, nor the transitions from them.

Equation (19) can be solved first, leading to $\boldsymbol{g}_n(s) = (s - \boldsymbol{R}_{nn})^{-1}\boldsymbol{p}_{n,0}$ and inserting this expression into the Eq. (21) gives

$$g(s, \boldsymbol{\iota}, \boldsymbol{c}, \boldsymbol{\pi}) = [\boldsymbol{R}_{wn}(s - \boldsymbol{R}_{nn})^{-1}\boldsymbol{p}_{n,0}]_{\boldsymbol{c}}, \quad \boldsymbol{c} \in S_w. \tag{22}$$

Please note that Eq. (22) is well defined for all values of s. In particular, in the limit $s \to 0$ even for a matrix $\boldsymbol{R}$ that has zero eigenvalues. It is intuitively clear that, contrary to $\boldsymbol{R}$, matrix $\boldsymbol{R}_{nn}$ does not have zero eigenvalues: as time goes on, all probability accumulates in S_w and S_t spaces (see Fig. 3).

The only difficulty with Eq. (22) is the partitioning of the full configuration space into S_n, S_w, and S_t. The algorithm for carrying out such partitioning works as follows. Assuming that the configuration space has been generated [Fig. 3, panel (a)] one starts from the window states that are easy to identify. Assume that the graph is elastic. All the lines arriving into the window states, together with the sites they are attached to, are pulled into the window states, one by one. Eventually, the whole graph collapses into the very simple structure shown in panel (b). All states that are drawn in the pool of w_1, w_2, etc. form S_n and the states left form S_t.

Once $g(s, \boldsymbol{\iota}, \boldsymbol{c}, \boldsymbol{\pi})$ is found one can proceed with the calculation of the moments $\gamma_k^p(\boldsymbol{\iota}, \boldsymbol{\pi})$. These can be obtained by taking derivatives of Eq. (17) with regard to s and setting $s = 0$ at the end: it can be seen easily from Eq. (15) that

$$\gamma_k^p(\boldsymbol{\iota}, \boldsymbol{\pi}) = (-)^p \lim_{s \to 0} \partial_s^p \Gamma_k(s, \boldsymbol{\iota}, \boldsymbol{\pi}), \tag{23}$$

where ∂_s denotes derivative over s. Using Eqs. (23) and (17) leads to

$$\gamma_k^{(p)}(\boldsymbol{\iota}, \boldsymbol{\pi}) = \sum_{\boldsymbol{c} \neq \boldsymbol{\iota}} w(\boldsymbol{c}, \pi_k) g^{(p)}(\boldsymbol{\iota}, \boldsymbol{c}, \boldsymbol{\pi}) + \sum_{m=1, \eta}^{m \neq k} \sum_{\boldsymbol{c} \neq \boldsymbol{\iota}} w(\boldsymbol{c}, \pi_m) \sum_{q=0,p} \binom{p}{q} g^{(p)}(\boldsymbol{\iota}, \boldsymbol{c}, \boldsymbol{\pi}) \gamma_k^{(p-q)} \times (\boldsymbol{c}/\pi_m, \boldsymbol{\pi}/\pi_m). \tag{24}$$

By definition, $g^{(p)}(\boldsymbol{\iota}, \boldsymbol{c}, \boldsymbol{\pi}) \equiv (-)^p \lim_{s \to 0} \partial_s^p g(s, \boldsymbol{\iota}, \boldsymbol{c}, \boldsymbol{\pi})$, which after using Eq. (22) leads to

$$g^{(p)}(\boldsymbol{\iota}, \boldsymbol{c}, \boldsymbol{\pi}) = (-)^{(p+1)} p\,! \,[\boldsymbol{R}_{wn}\boldsymbol{R}_{nn}^{-(p+1)}\boldsymbol{p}_{n,0}]_{\boldsymbol{c}}. \tag{25}$$

Equations (24) and (25) are the central result of this section. They determine all the moments. For example, once $\gamma_k^{(p)}(\boldsymbol{\iota}, \boldsymbol{\pi})$ $p = 0,1$ are found the average reaction times for each task are given by

$$\tau_k(\boldsymbol{\iota}, \boldsymbol{\pi}) = \frac{\gamma_k^{(1)}(\boldsymbol{\iota}, \boldsymbol{\pi})}{\gamma_k^{(0)}(\boldsymbol{\iota}, \boldsymbol{\pi})}, \tag{26}$$

where $k = 1, \ldots, \eta$. The term $\gamma_k^{(0)}(\boldsymbol{\iota}, \boldsymbol{\pi})$ ensures that the statistics is done only for instances where task was achieved. The percentage of cases when this happened is given by $\gamma_k^{(0)}(\boldsymbol{\iota}, \boldsymbol{\pi})$, which is either equal to or less than 1. The numerical implementation of Eqs. (24) and (25) is straightforward and gives the *exact* values for $\boldsymbol{\tau}$.

VI. ROGE ENSEMBLE: DESCRIBING PERFORMANCE OF ORGANISM IN TERMS OF THE SINGLE VARIABLE ν

To illustrate the workings of the method that are a relatively simple example will be studied with two particles types and two containers connected with the tube of length l. The umber of configurations increases exponentially with total particle number and to control the calculation the upper limit on this number N_p^* is set.

The structure of the organisms in the ROGE ensemble is defined as follows. For each organism in the ensemble an unique choice is made for (i) the total number of A and B molecules, (ii) the reactivity matrix $\boldsymbol{\Lambda}$, (iii) the catalytic activity matrix $\boldsymbol{K}$, (iv) the inject pattern $\boldsymbol{\iota}$ and, (v) the list of tasks monitored $\boldsymbol{\pi}$. For all organisms geometry is kept fixed (e.g., the size of containers and the length of the tube connecting them).

Please note that there are two symmetries in the problem, the one that originates from the relabeling of particles, and another one that has to do with the relabeling of containers. Two organisms are said to be *equivalent* if they can be related by these symmetries. Special care is taken to eliminate the organism that is equivalent to the one already in the list.

We start with the situation where the total number of particles $N_p^* = n_{A,1} + n_{A,2} + n_{B,1} + n_{B,2}$ in the system equals 1. Also, we consider only organisms with reactions $A \to B$ and B

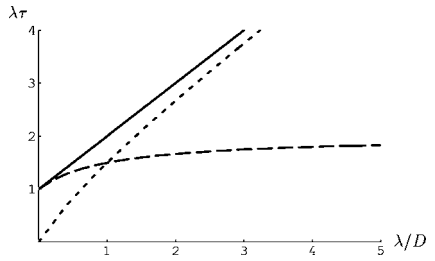

FIG. 4. The dependence of τ on λ/D for o_1 (dotted line), o_2 (dashed), and o_3 (solid). All quantities plotted are dimensionless.

$\rightarrow A$, both with the rate λ. One can see that, for a given reaction scheme, and with a constraint $N_p^*=1$, only three choices for $\boldsymbol{\iota}$ and $\boldsymbol{\pi}$ are possible: $\boldsymbol{\iota}_1$, $\boldsymbol{\pi}_1=[A]-[\,]$, $[\,]-[A]$; $\boldsymbol{\iota}_2$, $\boldsymbol{\pi}_2=[A]-[\,]$, $[B]-[\,]$; $\boldsymbol{\iota}_3$, $\boldsymbol{\pi}_3=[A]-[\,]$, $[\,]-[B]$. This leads to the three organisms o_1, o_2, and o_3.

All organisms are such that one A particle is injected in the container C_1 and only one task is monitored. In the case of organism o_1 the goal is to synthesize one A molecule in the container C_2, in the case of o_2 one B molecule should be synthesized in C_1, while in the case of o_3 one B molecule should be created in C_2. The expressions for τ of o_1, o_2, and o_3 can be found using Eqs. (24)–(26) leading to values $(2D+\lambda)/[D(D+\lambda)]$, $(D+2\lambda)/[\lambda(D+\lambda)]$, and $1/D+1/\lambda$, respectively.

The dependence of τ on $\lambda/D\sim l^2$ is depicted in Fig. 4. All three organisms achieve their tasks faster in the compact geometries since τ gets smaller when $l\rightarrow 0$. o_1 functions by transporting one A particle from C_1 to C_2. It is intuitively clear that this happens faster when containers are close. One can analyze o_3 in the similar way. For o_2 the task can be achieved without transport and the curve depicting τ for o_2 differs significantly from the ones for o_1 and o_3 when $l\rightarrow\infty$.

The question is whether it is possible to present information conveyed from Fig. 4 in a more compact way? To achieve this goal it is useful to consider following quantity:

$$\nu=\frac{\|\boldsymbol{\tau}_n\|}{\|\boldsymbol{\tau}_0\|} \tag{27}$$

where $\|.\|$ denotes the Euclidean norm of the vector, $\boldsymbol{\tau}_n$ and $\boldsymbol{\tau}_0$ are given by $\boldsymbol{\tau}$ calculated for networklike and compact geometries with jump rates D_n and D_0 such that $D_n\sim\lambda$ and $D_0\gg D_n$, $\lambda,\xi\lambda$. Using similar reasoning the ν can be defined for generic network having more than two containers. In such a way one can compare the extended and compact geometries of the given fixed network structure and express a comparison through one variable ν.

In the following the ν will be refereed to as the *speed* of a reaction. $\nu<1$ is an indication that the organisms accomplish tasks faster in a networklike geometry, while $\nu>1$ shows that the organism draws the most benefit from a compact geometry. Please note, all organisms considered in Fig. 4 have $\nu>1$.

VII. ROGE ENSEMBLE: CLASSIFICATION OF THE REACTION SCHEMES USING THE SPEED OF REACTION ν

Figure 5 depicts the results of the classification of a large number of organisms in five ROGE ensembles with $N_p^*=1,2,3,4,5$. Organisms are generated by loops over $\boldsymbol{\Lambda}$, $\boldsymbol{K}$, $\boldsymbol{\iota}$, and $\boldsymbol{\pi}$. This procedure leads to ensembles with 380, 2840, 12 020, 37 920, and 99 240 organisms. After eliminating equivalences one ends up with smaller numbers 95, 730, 3025, 9560, and 24 890. These numbers are hard to predict and they have to be generated by computer.

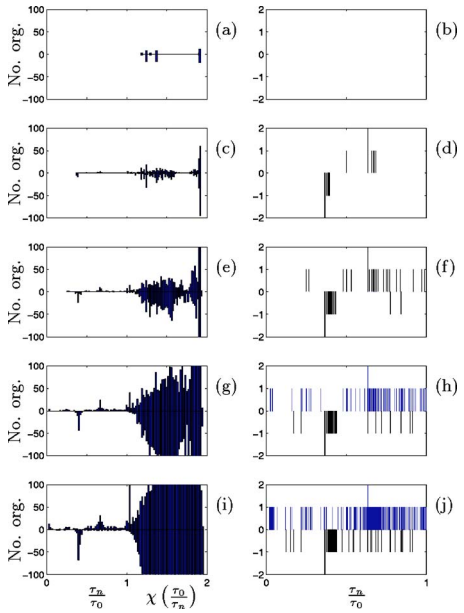

FIG. 5. (Color online) Classification of organisms in the ROGE ensemble. ν was calculated with $D_n=1\ s^{-1}$, $D_0=3125\ s^{-1}$, $\lambda=1\ s^{-1}$, and $\xi=100$. Panels (a), (c), (e), (g), and (i) are histograms that depict groups with similar reaction speed ν. There are 100 classes of width 0.01 for ν from 1 to 2. For $\nu>1$, instead of ν, the value obtained from $\chi(\nu)=2-\ln 2/\ln(1+\nu)$ is used. The function χ monotonically grows with ν and maps infinite interval $[1,\infty)$ onto the finite one $[1,2]$. In addition, this particular form for χ reveals more details in the region near $\nu=1$. Panels (b), (d), (f), (h), and (j) are discrete spectra (no histogram) for region $\nu\in[0,1]$. Panels in the same row have same value for the total number of particles in the system N_p^*: (a) and (b) $N_p^*=1$, (c) and (d) $N_p^*=2$, (e) and (f) $N_p^*=3$, (g) and (h) $N_p^*=4$, (i) and (j) $N_p^*=5$. A negative value for the number of organisms indicates that an organism with a particular value of ν contains at least one reaction that is inhibited.

There are no organisms in the $N_p^*=1$ class that benefit from the structured geometry since the histogram in panel (b) is empty. All organisms have $\nu>1$ as can be seen from panel (a). Only after more than one molecule appears in the system, catalytic influences start to play the role, and organisms that benefit from the networklike structure appear [see panels (c) and (d) in Fig. 5]. This clearly shows that when various reaction steps start influencing each other there is a need for structured geometry. This is a very important finding.

The best performer in the $N_p^*=2$ class is given in Table I, denoted by $o_{i,2}$, together with a couple of second best performers denoted by $o_{ii,2}$. The degeneracy in ν of $o_{i,2}$ comes from the fact that the same enhancement and reduction factor is used for positive and negative catalytic influence.

One can understand intuitively why $o_{i,2}$ runs faster in the networklike geometry. We focus on the particular case of $o_{i,2}$ where the goal is to synthesize two B molecules in the con-

TABLE I. List of the best performers in the ROGE ensemble (first row). A couple of second best performers are also shown (second row). The last row contains organisms that are obtained by slightly perturbing winners from the first row.

$N_p^*=2$	$N_p^*=3$	$N_p^*=4$	$N_p^*=5$
$(o_{i,2})$	$(o_{i,3})$	$(o_{i,4})$	$(o_{i,5})$
$A\xrightarrow{-A}B, B\xrightarrow{+A}A(R_1)$	$A\xrightarrow{+A}B(R_3)$	$A\xrightarrow{+A}B(R_3)$	$A\xrightarrow{+A}B(R_3)$
$\boldsymbol{\iota}=[A]-[B]$	$\boldsymbol{\iota}=[A]-[2A]$	$\boldsymbol{\iota}=[A]-[3A]$	$\boldsymbol{\iota}=[2A]-[3A]$
$\boldsymbol{\pi}=[2B]-[\ ]$ or $[\ ]-[2B]$	$\boldsymbol{\pi}=[2A]-[B]$	$\boldsymbol{\pi}=[3A]-[B]$	$\boldsymbol{\pi}=[4A]-[B]$
$\boldsymbol{\tau}_n=[18.55]-[\ ]$	$\boldsymbol{\tau}_n=[0.242]-[0.0355]$	$\boldsymbol{\tau}_n=[0.021]-[0.01]$	$\boldsymbol{\tau}_n=[0.014]-[0.00063]$
$\boldsymbol{\tau}_0=[50.91]-[\ ]$	$\boldsymbol{\tau}_0=[0.000219]-[0.979]$	$\boldsymbol{\tau}_0=[0.00045]-[0.95]$	$\boldsymbol{\tau}_0=[0.010]-[0.91]$
$\nu=0.364$	$\nu=0.250$	$\nu=0.0248$	$\nu=0.0192$
$(o_{ii,2})$	$(o_{ii,3})$	$(o_{ii,4})$	$(o_{ii,5})$
$A\xrightarrow{-B}B, B\xrightarrow{+A}A(R_2)$	$R_3, \boldsymbol{\iota}=[\ ]-[3A]$	$R_3, \boldsymbol{\iota}=[2A]-[2A]$	$R_3, \boldsymbol{\iota}=[2A]-[3A]$
$\boldsymbol{\iota}=[A]-[B], \boldsymbol{\pi}=[2B]-[\ ]$	$\boldsymbol{\pi}=[2A]-[B], \nu=0.268;$	$\boldsymbol{\pi}=[3A]-[B], \nu=0.0279;$	$\boldsymbol{\pi}=[4A,B]-[\ ], \nu=0.0219;$
or $[\ ]-[2B], \nu=0.368$	$R_1, \boldsymbol{\iota}=[2A]-[B]$	$R_3, \boldsymbol{\iota}=[\ ]-[4A]$	$R_3, \boldsymbol{\iota}=[A]-[4A]$
$R_1, \boldsymbol{\iota}=[\ ]-[2A],$	$\boldsymbol{\pi}=[A]-[2B]$	$\boldsymbol{\pi}=[3A]-[B], \nu=0.0358$	$\boldsymbol{\pi}=[4A]-[B], \nu=0.0305$
$\boldsymbol{\pi}=[2B]-[\ ], \nu=0.386$ $R_3, \boldsymbol{\iota}=[\ ]-[2A],$	$R_2, \boldsymbol{\iota}=[2A]-[B]$		
$\boldsymbol{\pi}=[A]-[B], \nu=0.500$	$\boldsymbol{\pi}=[2B]-[A]$ or $[\ ]-[A,2B]$		
	$\nu\approx 0.386$		
$(o_{*,2})$	$(o_{*,3})$	$(o_{*,4})$	$(o_{*,5})$
R_1 or $R_3, \boldsymbol{\iota}=[\ ]-[2A]$	$R_3, \boldsymbol{\iota}=[A]-[2A]$	$R_3, \boldsymbol{\iota}=[A]-[3A]$	$R_3, \boldsymbol{\iota}=[2A]-[3A]$
$\boldsymbol{\pi}=[2A]-[\ ], \nu=3249$ or 418;	$\boldsymbol{\pi}=[3A]-[\ ], \nu=21.8$	$\boldsymbol{\pi}=[4A]-[\ ], \nu=17.5$	$\boldsymbol{\pi}=[5A]-[\ ], \nu=10.4$

tainer C_1. Due to the initial presence of molecule A in container C_1, it is very likely that the B molecule will be converted into an A molecule, when A and B meet in the same container. Once there are two A molecules in the system the trouble starts. Even if the reaction $A\rightarrow B$ happens, and chance for this is really small due to the negative catalytic influence of A on such reaction, B will be converted back to A immediately (due to the positive catalytic influence of another A molecule on the $B\rightarrow A$ reaction). In principle, conversion of AB into $2B$ has no chance occurring in a reasonable time when there is only one container. The antagonistic catalytic influences just discussed are best handled in a networklike geometry. In such a case the synthesis of the molecules can be done in separate containers. With two containers there is always a chance that the antagonistic influences will be reduced. For example, in this case the processes $A\rightarrow B$ can happen fast given that damage inflicting an A molecule is in another container.

Also, it is naive to think that organisms containing reactions with solely inhibitory catalytic influence perform best in a networklike structure. This is clearly not the case. The winning organisms $o_{i,2}$ are constructed from one reaction with positive $B\rightarrow^{+A}A$ and another reaction $A\rightarrow^{-A}B$ with a negative catalytic influence. Furthermore, Fig. 5 shows plenty of other cases. Actually, the completely opposite is possible. There are many organisms in the histogram plot with $\nu>1$ that contain at least one reaction with a negative catalytic influence and these organisms perform best in a compact geometry.

The best performer in the $N_p^*=3$ class is given in Table I, denoted by $o_{i,3}$. A couple of the second best performers are also shown and labeled $o_{ii,3}$. When more than two molecules appear in the system, a completely different organism appears as the winner. There is a sharp transition in the character of winners. Both the reaction type and inject and task patterns are different in $o_{i,3}$ and $o_{i,2}$. The winners in classes $N_p^*=4$ and $N_p^*=5$ are similar to $o_{i,3}$.

Table I shows how difficult it is to have any intuition about the structure of best performers. For example, the inject patterns of $o_{i,3}$, $o_{i,4}$, and $o_{i,5}$ form a list $[A]-[2A]$, $[A]-[3A]$, and $[2A]-[3A]$ (surprisingly not $[A]-[4A]$). Also, the last row in Table I contains organisms with a slightly modified inject or task patterns where the original form is taken from the best performer. Comparing $o_{i,3}$ and $o_{*,3}$, $o_{i,4}$, and $o_{*,4}$, and finally $o_{i,5}$ with $o_{*,5}$ shows that small alternation in the task pattern, obtained by moving one B particle from C_2 into C_1, deteriorates the performance leading to $\nu>1$. Another example, can be obtained from comparison of $o_{i,3}$ with $o_{*,2}$. Both the inject and task patterns have been altered in $o_{i,3}$. This change is motivated by a sequence of organisms in the first row of Table I, when read from right to left. *A priori*, the organism $o_{*,2}$ could be considered to have $\nu<1$, however, this is not the case. The actual value for $\nu=418$ is (lot) larger than 1.

VIII. DISCUSSION

We introduced what we might call a generic model for the study of chemical reactions in structured spaces, based on a simple way of incorporating interplay between transport, chemical reactions, and geometry. A number of different chemical reactions were studied and their performance compared. To compare organisms we used a measure of relative performance expressed through the single variable ν, the ratio of the average execution times in stretched and compact geometries.

To calculate ν is not easy since the dynamics is stochastic. The computer simulation is a straightforward way to obtain ν. However, one needs unrealistically large number of runs ($\sim$100 000) in order to gain reasonable accuracy in ν for one

organism. An alternative method was suggested, where average times are calculated using the concept of the first passage time. This method is exact and much more efficient computationally and should be used when possible.

Which types of chemical reactions draw the most benefit from structured spaces? In an attempt to answer this question two schemes were formulated ROGE and GORE, while examples were only given for ROGE. The variable ν was used to classify the performance of various organisms in the geometry consisting of two containers connected by the tube. The results of the analysis can be found in Fig. 5 and Table I and two main findings are as follows.

(1) The interplay between the geometry and reaction scheme becomes important only when the reaction steps start influencing each other. The reaction pathways containing *antagonistic* reaction steps that slow down the production of the final product require networklike geometry to run fast. The dangerous reaction steps have to be isolated in the separate regions of space, and additional time has to be spent to move reactants there. However, the overall reaction time might get shorter since the other reactions speed up.

(2) Intuition does not help much and one really has to do numerical analysis in order to extract the best performer in a given class. The whole triple consisting of the reaction, inject pattern, and task pattern has to be considered simultaneously. There are a couple of reasons for this. First, the performance is extremely sensitive to the details of the inject and task patterns. Second, antagonistic catalytic influences are hard to identify since the role of the reactions with positive and negative (inhibitory) catalytic influence is symmetric.

The method suggested and the simple examples studied provide insights relevant for a number of topics ranging from the understanding of physiochemical processes in the living cell [33–36,39–49], biological evolution [50–56], toward chemical engineering and biotechnology [19–25].

(i) The moment method is a *quantitative* scheme that can be used to investigate temporal and spatial synchronization of the chemical reactions in the living cell [33,39]. These are hotly debated issues.

(ii) This study suggest another way of approaching cytoarchitecture [35,36]. For example, it is assumed that the inner space of the mitochondrion is structured in order to attain a higher surface of the inner membrane. The present study suggests the possibility of an additional mechanism, the presence of antagonistic catalytic influences.

(iii) Fairly little has been done in understanding the role of geometry and spatial organization played in the process of biological evolution. There is already some pioneering work in this area [52–56]. The present study could impact some progress in this direction.

(iv) There is a tendency within chemical engineering to move away from bulk geometry toward structured spaces. The interesting experimental work on these topics can be found in Refs. [19–25]. It is possible that, among other things, the structures studied in these experiments will find its use as a device to efficiently run reactions with antagonistic catalytic influences. The method suggested could be used to identify interesting reactions.

The setup suggested here is generic. There are many possible ways of extending the present the analysis. For example, at present the focus is on a small number of particles and stochastic dynamics. When the number of particles in the system increases the present scheme cannot be carried out. In such a case the mean field description becomes valid. The present analysis could be easily repeated in such a setup. The transport between the containers can be treated in a better way. Instead of focusing on the average execution time $\boldsymbol{\tau}$ one can easily look at the noise $\boldsymbol{\sigma}$ or the combination of the two. The GORE ensemble should be explored in a lot more detail. These issues will be addressed in future work.

ACKNOWLEDGMENTS

I would like to thank Professor Owe Orwar and members of his group for fruitful discussions that provided motivation for this work and for warm hospitality during the Särö meeting 2005. The financial support of Professor Owe Orwar is greatly acknowledged.

[1] R. J. Bagley and J. D. Farmer, in *Artificial Life II*, edited by C. G. Langton, C. Taylor, J. D. Farmer, and S. Rasmussen (Addison-Wesley, Reading, MA, 1992), pp. 93–140.
[2] R. J. Bagley, J. D. Farmer, and W. Fontana, in *Artificial Life II*, edited by C. G. Langton, C. Taylor, J. D. Farmer, and S. Rasmussen (Addison-Wesley, Reading, MA, 1992), pp. 141–158.
[3] J. D. Farmer, S. A. Kauffman, and N. H. Packard, Physica D **22**, 50 (1986).
[4] S. A. Kauffman, J. Theor. Biol. **119**, 1 (1986).
[5] P. F. Stadler, W. Fontana, and J. H. Miller, Physica D **63**, 378 (1993).
[6] P. Schuster, Physica D **22**, 100 (1986).
[7] F. Slanina and M. Kotrla, Phys. Rev. Lett. **83**, 5587 (1999).
[8] S. Jain and S. Krishna, Phys. Rev. Lett. **81**, 5684 (1998).
[9] E. Kotomin and V. Kuzovkov, Rep. Prog. Phys. **55**, 2079 (1992).
[10] E. Kotomin and V. Kuzovkov, *Comprehensive Chemical Kinetics*, edited by R. G. Compton and G. Hancock (Elsevier, New York, 1996), Vol. 34.
[11] *Comprehensive Chemical Kinetics*, edited by C. H. Bamford, C. F. H. Tipper, and R. G. Compton (Elsevier, New York, 1985), Vol. 25.
[12] E. Kotomin and V. Kuzovkov, *Comprehensive Chemical Kinetics*, edited by R. G. Compton and G. Hancock (Elsevier, New York, 1996), Vol. 34.
[13] A. S. Mikhailov, Phys. Rep. **184**, 307 (1989).
[14] A. A. Ovchinnikov, S. F. Timashev, and A. A. Belyy, *Kinetics of Diffusion Controlled Chemical Processses* (Nova Science, Commack, NY, 1989).
[15] D. McQuarrie, J. Appl. Probab. **4**, 413 (1967).
[16] P. Clifford, N. J. B. Green, and M. J. Pilling, J. Phys. Chem. **86**, 1318 (1982).

[17] R. F. Khairutdinov and N. Serpone, Prog. React. Kinet. **21**, 1 (1996).
[18] Z. Konkoli, A. Karlsson, and O. Orwar, J. Phys. Chem. B **107**, 14 077 (2003).
[19] M. Karlsson, M. Davidson, R. Karlsson, A. Karlsson, J. Bergenholtz, Z. Konkoli, A. Jesorka, T. Lobovkina, J. Hurtig, M. Voinova, and O. Orwar, Annu. Rev. Phys. Chem. **55**, 613 (2004).
[20] M. Karlsson, K. Sott, M. Davidson, A. S. Cans, P. Linderholm, D. Chiu, and O. Orwar, Proc. Natl. Acad. Sci. U.S.A. **99**, 11 573 (2002).
[21] A. Karlsson, R. Karlsson, M. Karlsson, A. S. Cans, A. Stromberg, F. Ryttsen, and O. Orwar, Nature (London) **409**, 150 (2001).
[22] M. Karlsson, K. Nolkrantz, M. J. Davidson, A. Stromberg, F. Ryttsen, B. Akerman, and O. Orwar, Anal. Chem. **72**, 5857 (2000).
[23] J. P. Laplante, M. Pemberton, A. Hjelmfelt, and J. Ross, J. Phys. Chem. **99**, 10 063 (1995).
[24] A. Hjelmfelt and J. Ross, J. Phys. Chem. **97**, 7988 (1993).
[25] A. Hjelmfelt, F. W. Schneider, and J. Ross, Science **260**, 335 (1993).
[26] K. Akingbehin, BioSystems **35**, 223 (1995).
[27] K. Akingbehin and M. Conrad, J. Parallel Distrib. Comput. **6**, 245 (1989).
[28] M. Conrad, Eur. J. Oper. Res. **30**, 280 (1987).
[29] K. G. Kirby and M. Conrad, Physica D **22**, 205 (1986).
[30] K. G. Kirby and M. Conrad, Bull. Math. Biol. **46**, 765 (1984).
[31] R. Kampfner and M. Conrad, Bull. Math. Biol. **45**, 931 (1983).
[32] R. Kampfner and M. Conrad, Bull. Math. Biol. **45**, 969 (1983).
[33] H. Kuthan, Prog. Biophys. Mol. Biol. **75**, 1 (2001).
[34] L. Stryer, *Biochemistry* (Freeman, New York, 1992).
[35] K. Luby-Phelps, Int. Rev. Cytol. **192**, 189 (2000).
[36] L. Pagliaro, Int. Rev. Cytol. **192**, 303 (2000).
[37] D. T. Gillespie, J. Comput. Phys. **22**, 403 (1976).
[38] D. T. Gillespie, J. Phys. Chem. **81**, 2340 (1977).
[39] G. L. Nelsestuen, Chem. Phys. Lipids **101**, 37 (1999).
[40] T. Ganti, BioSystems **7**, 15 (1975).
[41] M. L. Simpson, G. S. Sayler, J. T. Fleming, and B. Applegate, Trends Biotechnol. **19**, 317 (2001).
[42] A. Mikhailov and B. Hess, J. Phys. Chem. **100**, 19 059 (1996).
[43] P. Stange, A. S. Mikhailov, and B. Hess, J. Phys. Chem. B **102**, 6273 (1998).
[44] P. Stange, A. S. Mikhailov, and B. Hess, J. Phys. Chem. B **103**, 6111 (1999).
[45] P. Stange, D. Zanette, A. S. Mikhailov, and B. Hess, Biophys. Chem. **79**, 233 (1999).
[46] P. Stange, A. S. Mikhailov, and B. Hess, J. Phys. Chem. B **104**, 1844 (2000).
[47] H. Wang, Q. Quyang, and Y. Lei, J. Phys. Chem. B **105**, 7099 (2001).
[48] K. Sun and Q. Ouyang, Phys. Rev. E **64**, 026111 (2001).
[49] H. Qian and M. Qian Phys. Rev. Lett. **84**(10), 2271 (2000).
[50] M. Calvin, *Chemical Evolution: Molecular Evolution Towards the Origin of Living Systems on the Earth and Elsewhere* (Claredon Press, Oxford, 1969).
[51] M. V. Volkenstein, *Physical Approaches to Biological Evolution*, (Springer-Verlag, New York, 1994).
[52] C. Langton, Physica D **22**, 120 (1986).
[53] C. Furusawa and K. Kaneko, Artif. Life **4**, 79 (1998).
[54] Z. Vespalcova, A. V. Holden, and J. Brindley, Phys. Lett. A **197**, 147 (1995).
[55] N. Ono and T. Ikegami, J. Theor. Biol. **206**, 243 (2000).
[56] M. Boerljist and P. Hogeweg, Physica D **48**, 17 (1992).